



# Journal of Applied and Computational Mechanics



Research Paper

## Discretization of the 2D Convection–Diffusion Equation Using Discrete Exterior Calculus

Marco A. Noguez<sup>1</sup>, Salvador Botello<sup>2</sup>, Rafael Herrera<sup>3</sup>, Humberto Esqueda<sup>4</sup>

<sup>1</sup> Centro de Investigación en Matemáticas A.C. CIMAT, Jalisco S/N, Col. Valenciana, Guanajuato, Gto, 36023, México, Email: marco.noguez@ciamat.mx

<sup>2</sup> Centro de Investigación en Matemáticas A.C. CIMAT, Jalisco S/N, Col. Valenciana, Guanajuato, Gto, 36023, México, Email: botello@ciamat.mx

<sup>3</sup> Centro de Investigación en Matemáticas A.C. CIMAT, Jalisco S/N, Col. Valenciana, Guanajuato, Gto, 36023, México, Email: rherrera@ciamat.mx

<sup>4</sup> Centro de Investigación en Matemáticas A.C. CIMAT, Jalisco S/N, Col. Valenciana, Guanajuato, Gto, 36023, México, Email: esqueda@ciamat.mx

Received July 04 2020; Revised August 24 2020; Accepted for publication August 24 2020.

Corresponding author: M.A. Noguez (marco.noguez@ciamat.mx)

© 2020 Published by Shahid Chamran University of Ahvaz

**Abstract.** While the Discrete Exterior Calculus (DEC) discretization of the diffusive term of the Transport Equation is well understood, the DEC discretization of the convective term, as well as its stabilization, is an ongoing area of research. In this paper, we propose a local discretization for this term based on DEC and geometric arguments, considering the particle velocity field prescribed at the vertices of the primal mesh. This formulation is similar to that of the Finite Element Method with linear interpolation functions (FEM) and can be stabilized using known stabilization techniques, such as Artificial Diffusion. Using this feature, numerical tests are carried out on simple stationary and transient problems with domains discretized with coarse and fine simplicial meshes to show numerical convergence.

**Keywords:** Discrete Exterior Calculus, Finite Element Analysis, Transport Equation, Compressible and Incompressible Flow, Convection, Advection, Diffusion.

### 1. Introduction

Discrete Exterior Calculus (DEC) is a relatively new numerical method for solving partial differential equations (PDE's), based on the discretization of the Exterior Differential Calculus theory of Cartan [1]. It was first proposed by A. Hirani in his PHD thesis [2] and its accuracy has been studied in [3 - 5]. It has been applied to solve Darcy's equation [6], Navier-Stokes and Poisson's equations [7 - 9], plasticity and failure of isotropic materials [10], and the transport equation with incompressible flow for advection-dominated problems [11]. In particular, the authors of [11] showed that, in simple cases, the system of equations resulting from DEC are equivalent to other numerical methods, such as the Finite Differences and Finite Volume methods, leading to a stable upwind DEC variation, which involves the Lie derivative, also discretized in [12].

The transport equation, or Convection-Diffusion equation, is a linear parabolic partial differential equation which models the transport of a scalar field due to diffusion and transport mechanisms (convection for heat transfer or advection for any substance) in a fluid in motion. This equation arises in several applications and studies (see [13 - 14] for example) as well as in engineering problems like air pollution and groundwater contamination, where the solute is transported by advection due to the particle velocity field, which usually depends on time and spatial coordinates. Analytic solutions for this equation have been studied in depth and remarkable advances had been made in the past few years, see for example [15 - 18]. Nevertheless, these solutions are commonly limited to simple scenarios such as 1D domains or steady-state problems and are highly dependent on initial and boundary conditions. Therefore, numerical approaches are usually preferred when tackling engineering problems.

Figure 1 shows a typical problem of groundwater contamination of a confined aquifer, where this equation is used to model the spatial and temporal distribution of the plume's concentration. Pollution might occur due to infiltration through the soil and/or the confining rock. The plume's form depends mainly on the ground water flow direction and magnitude, as well as the pollutant diffusion coefficient.

Commonly, this type of problems are advection-dominated problems, since the magnitude of the particle velocity is greater than the pollutant's diffusion coefficient, leading to numerical instabilities for most of the mesh-based numerical methods for solving PDE's. In such cases, stabilization techniques such as the Stream-Upwind/Petrov-Galerkin (SUPG) [19] and Galerkin/Least-Squares (GLS) [20] are employed. However, they may not be well suited for some problems and refining the mesh may yield numerical stabilization at a high computational cost. Thus, the importance of trying to develop efficient numerical scheme becomes evident.

In this paper, we propose a local DEC discretization of the Convection-Diffusion equation for compressible and incompressible flow. This formulation is developed based on DEC and "natural" geometric arguments, assuming the values of the particle velocity field are given at the nodes of the primal mesh, thus making it different from the discretization in [11]. Since our discretization on



the Convection-Diffusion equation will not involve discrete dual-to-primal Hodge star operators, it can be developed in a local manner similar to that of FEM (see [21]) together with its assembling technique, leading to an efficient implementation. Nevertheless, as it turns out, our discretization needs to be stabilized, a process we carry out by introducing Artificial Diffusion.

The rest of this article is organized as follows: In Section 2 we review some basic DEC concepts which are essential in the development of this proposal. In Section 3 we describe the procedure to compute the local DEC discretization matrix for the Transport Equation. In Section 4, we show some numerical results on simple domains to show numerical convergence, considering laminar, sinusoidal and rotational velocity fields. In Section 5 we present our conclusions. In the Appendix we present how the artificial diffusion is calculated.

## 2. Preliminaries

Since there exist various detailed accounts of Discrete Exterior Calculus ([2 - 12]) and the Convection-Diffusion equation does not involve discrete dual-to-primal Hodge star matrices, the whole discussion can be carried out in a local manner and we shall, therefore, recall the necessary concepts accordingly (see [21 - 22]).

### 2.1 Vector fields and differential 1-forms

A smooth vector field  $\underline{u}$  on an open domain  $\Omega \subset \mathbb{R}^2$  is a function that assigns a vector to each point  $(x, y) \in \Omega$ , i.e.

$$\underline{u}(x, y) = (u_1(x, y), u_2(x, y)) \in \mathbb{R}^2, \tag{1}$$

where the two functions  $u_1, u_2$  are smooth. We can construct a so-called *differential 1-form*  $\underline{u}^\flat$  using the dot product as follows. At each point  $(x, y) \in \Omega$

$$\underline{u}^\flat_{(x,y)}(Y_1, Y_2) := \underline{u}(x, y) \cdot (Y_1, Y_2) = u_1(x, y)Y_1 + u_2(x, y)Y_2, \tag{2}$$

where  $(Y_1, Y_2) \in \mathbb{R}^2$  is an arbitrary vector.

The *Hodge star* of the 1-form  $\underline{u}^\flat$  is defined by

$$(\star \underline{u}^\flat)_{(x,y)}(Y) := -u_2(x, y)Y_1 + u_1(x, y)Y_2, \tag{3}$$

which is reminiscent of a 90° rotation in 2D, and is associated to the vector field  $(-u_2, u_1)$ . The exterior derivative of the 1-form  $\underline{u}^\flat$  is defined by

$$(d\underline{u}^\flat)_{(x,y)}((Y_1, Y_2), (Z_1, Z_2)) := \left( \frac{\partial u_2}{\partial x} - \frac{\partial u_1}{\partial y} \right) \det \begin{pmatrix} Y_1 & Y_2 \\ Z_1 & Z_2 \end{pmatrix}, \tag{4}$$

for any  $(Y_1, Y_2), (Z_1, Z_2) \in \mathbb{R}^2$ . The exterior derivative of a 0-form or function  $\varphi$  is defined by

$$(d\varphi)_{(x,y)}(Y_1, Y_2) := \frac{\partial \varphi}{\partial x} Y_1 + \frac{\partial \varphi}{\partial y} Y_2, \tag{5}$$

a value equal to the dot product of the vector  $(Y_1, Y_2)$  with the gradient  $\nabla \varphi(x, y)$ .

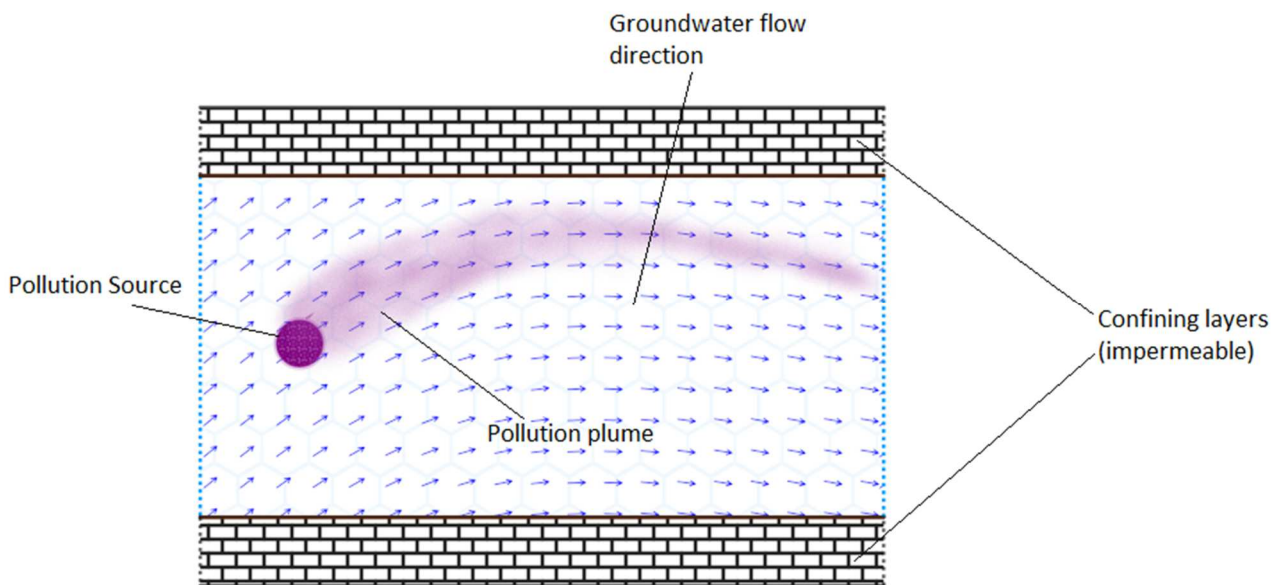


Fig. 1. Groundwater pollution of a confined aquifer. Solute is transported by advection and diffusion, creating a pollution plume.



## 2.2 From Vector Calculus to Exterior Differential Calculus

As described in [7], in order to develop a DEC discretization of a partial differential equation, we must first rewrite it in Exterior Differential Calculus notation. Since we are going to be dealing with the 2D convection-diffusion equation, we will need to substitute the following identities for the gradient, the divergence and the Laplacian operators (see [6] and [23] for a discussion about these identities and differential forms):

$$\begin{aligned}\nabla\varphi &= d\varphi, \\ \nabla\cdot\mathbf{u} &= \star d\star\mathbf{u}^\flat, \\ \nabla^2\varphi &= \star d\star d\varphi,\end{aligned}\quad (6)$$

where  $\varphi$  is a scalar function (or a 0-form),  $\mathbf{u}$  is a vector field,  $d$  is the exterior derivative and  $\star$  is the Hodge Star. Thus, by substituting eq. (6), the 2D isotropic homogeneous and stationary Convection-Diffusion equation:

$$\nabla\cdot(\varphi\mathbf{u}) = k\nabla^2\varphi + q, \quad (7)$$

can now be written in terms of Exterior Differential Calculus as follows:

$$\star d\star(\mathbf{u}^\flat\varphi) = k\star d\star d\varphi + q, \quad (8)$$

where  $\varphi$  is the scalar unknown function,  $\mathbf{u}$  is the particle velocity field,  $k$  is the diffusion coefficient and  $q$  is the external source. It is an elliptic equation which describes the transport of a scalar quantity due to transport processes known as convection, which is modeled by the left-hand side of eq. (7), and diffusion for mass transport, or heat conduction, which in turn, is modeled by the right-hand side of eq. (7).

## 2.3 Primal mesh

The next step is to discretize these operators over a given 2D well-centered primal mesh (simplicial complex). As in [21], the DEC discretization of the convection-diffusion equation can be carried out locally (element by element) and then assembled as in FEM. Thus, we will consider a single counterclockwise oriented triangle mesh  $[v_1, v_2, v_3]$ , such as the one shown in Fig. 2, formed by the vertices  $[v_1], [v_2], [v_3]$  and edges  $[v_1, v_2], [v_2, v_3], [v_3, v_1]$ .

## 2.4 Dual mesh

The dual cells for this mesh are defined as follows:

- The dual of the 2-dimensional triangle  $[v_1, v_2, v_3]$  is the 0-dimensional circumcenter  $[v_1, v_2, v_3]^\star$  of the triangle (see Fig. 3(a)).
- The dual of the 1-dimensional edges of the triangle is the 1-dimensional straight segment joining the mid-point of the edge and the triangle's circumcenter (e.g. the dual of the edge  $[v_1, v_2]$ , denoted as  $[v_1, v_2]^\star$  is shown in Fig 3(b)).
- The dual of the 0-dimensional vertices of the triangle is the 2-dimensional quadrilateral formed by the two mid-points of its adjacent edges, the vertex itself and the circumcenter (e.g. The dual of the vertex  $[v_1]$ , denoted as  $[v_1]^\star$  is the quadrilateral shown in Fig. 3(c)).

## 2.5 Primal and Dual Forms

As mentioned [23], the discretization of a differential  $k$ -form is done by its integration over all the  $k$ -dimensional elements of a primal (simplicial) mesh. In other words, the discretization of a  $k$ -form is a collection of values, one for each  $k$ -dimensional element of the mesh. For example, a 0-form  $\varphi$  is integrated over each vertex  $[v_i]$  of our primal mesh, which is equivalent to sample  $\varphi$  at the point  $v_i$ , i.e.:

$$\varphi_i := \int_{[v_i]} \varphi = \varphi(v_i), \quad i = 1, 2, 3. \quad (9)$$

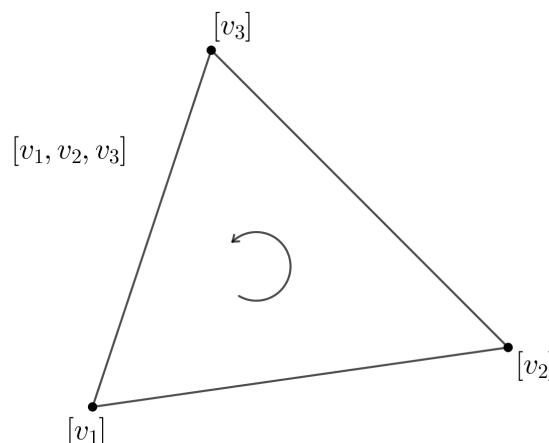


Fig. 2. Triangle  $[v_1, v_2, v_3]$ . Its edges are denoted as  $[v_1, v_2], [v_2, v_3], [v_3, v_1]$ .



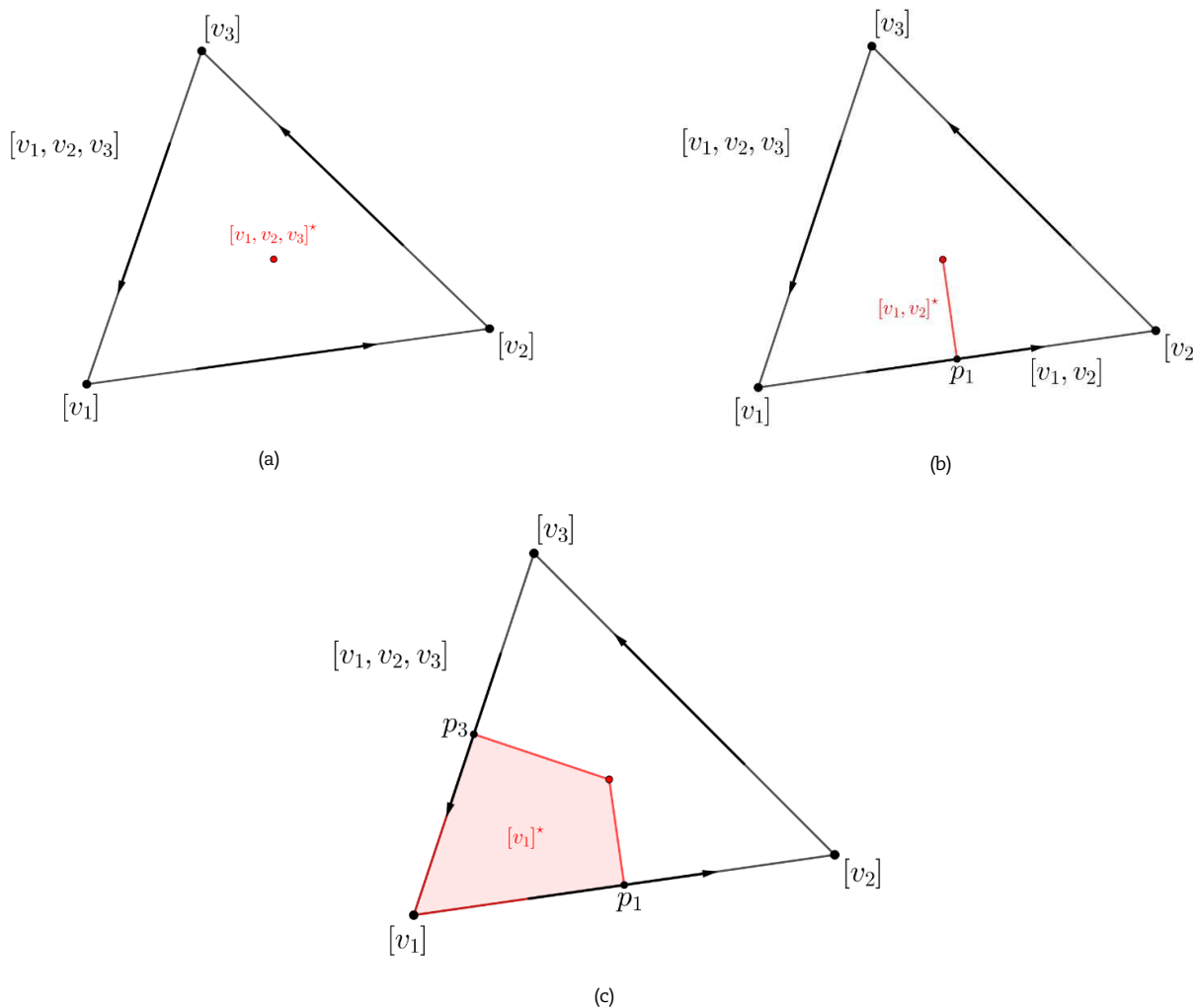


Fig. 3. Dual cells and edge orientation

In other words, we discretize  $\varphi$

$$\varphi \mapsto \tilde{\varphi} = \begin{pmatrix} \varphi_1 \\ \varphi_2 \\ \varphi_3 \end{pmatrix}. \tag{10}$$

Often we will denote the discretization of a field by adding a  $\sim$  to the given symbol. Similarly, a 1-form  $\underline{u}^b$  is integrated over the oriented edges of the mesh:

$$\tilde{\underline{u}}^b_{[v_i, v_j]} := \int_{[v_i, v_j]} \underline{u}^b = \int_0^1 \underline{u}(v_i + \tau(v_j - v_i)) \cdot (v_j - v_i) d\tau, \tag{11}$$

i.e. the value of a line integral for the vector field.

By analogy, dual  $k$  – forms can be calculated by integrating along the  $k$  – dimensional cells of the dual mesh.

**2.6 Discrete Exterior Derivative**

The discrete exterior derivative maps discrete primal  $k$  – forms to discrete primal  $(k + 1)$  – forms [7]. Thus, in order to compute the discrete exterior derivative, we calculate the analytical exterior derivative and integrate over the corresponding  $k$  – dimensional elements of the mesh. For example, consider a 0-form  $\alpha$  discretized over the vertices of the triangle shown in Fig. 2.:

$$\alpha \mapsto \tilde{\alpha} := \begin{pmatrix} \alpha_1 \\ \alpha_2 \\ \alpha_3 \end{pmatrix}, \tag{12}$$

since  $(d\alpha)$  1-form, we can integrate over the edges of the triangle, i.e.

$$(\tilde{d\alpha})_{[v_i, v_j]} = \int_{[v_i, v_j]} d\alpha, \quad i, j = 1, 2, 3; i \neq j \tag{13}$$



and, using the Stokes Theorem, one has

$$(\widetilde{d\alpha})_{[v_i, v_j]} = \int_{[v_i, v_j]} d\alpha = \int_{[v_i]}^{\alpha_j} - \alpha_i \quad i, j = 1, 2, 3; i \neq j \tag{14}$$

Thus, we can encode the local exterior derivative in matrix form as

$$D_{0,1} = \begin{bmatrix} -1 & 1 & 0 \\ 0 & -1 & 1 \\ 1 & 0 & -1 \end{bmatrix}, \tag{15}$$

where the subscript  $D_{0,1}$  means we are taking the exterior derivative of a primal 0-form and obtaining a primal 1-form. Finally, the exterior derivative which maps dual  $k$  – forms to dual  $(k + 1)$  – forms,  $D^*$  satisfies:

$$D_{(n-p), (n-p)+1}^* = (-1)^p D_{(p-1), p}^T, \tag{16}$$

where  $n$  is the dimension of the mesh. For example, in 2D, the dual discrete exterior derivative  $D_{1,2}^*$  is equal to  $-D_{0,1}^T$ .

### 2.7 Discrete Hodge Star

As mentioned in [7], the discrete Hodge Star ( $\star$ ) maps primal  $k$  – forms to dual  $(n - k)$  – forms, and is defined as

$$\star \alpha_i = \frac{|\alpha_i^*|}{|\alpha_i|} \widetilde{\alpha}_i, \tag{17}$$

where  $\widetilde{\alpha}_i$  is the discrete value of a primal  $k$  – form  $\alpha$  over the  $k$  – dimensional  $i_{th}$  – element  $\sigma_i$  and  $\sigma_i^*$  is its corresponding dual cell. The symbol  $|\cdot|$  denotes the unsigned volume of the cell (the volume of a vertex is 1 by convention). Since the discrete Hodge Star multiplies a discrete  $k$  – form by a ratio of volumes of primal and dual cells, it can be encoded as a diagonal matrix. In two dimensions, we have two discrete Hodge Star matrices, one relating primal 1-forms to dual 1-forms, and another one relating primal 0-forms to dual 2-forms. The first one is given by (see Fig. 4(a)):

$$M_{1,1} = \begin{bmatrix} \frac{|[v_1, v_2]^*|}{|[v_1, v_2]|} & 0 & 0 \\ 0 & \frac{|[v_2, v_3]^*|}{|[v_2, v_3]|} & 0 \\ 0 & 0 & \frac{|[v_3, v_1]^*|}{|[v_3, v_1]|} \end{bmatrix}, \tag{18}$$

where the subscript means that we are mapping discrete primal 1-forms to discrete dual 1-forms. Similarly, the second Hodge Star matrix discretization is given by (see Fig.4(b))

$$M_{0,2} = \begin{bmatrix} \frac{|[v_1]^*|}{|[v_1]|} & 0 & 0 \\ 0 & \frac{|[v_2]^*|}{|[v_2]|} & 0 \\ 0 & 0 & \frac{|[v_3]^*|}{|[v_3]|} \end{bmatrix}, \tag{19}$$

The inverse of  $M_{0,2}$  is the matrix  $M_{2,0}$  that maps discrete dual 2-forms to discrete primal 0-forms.

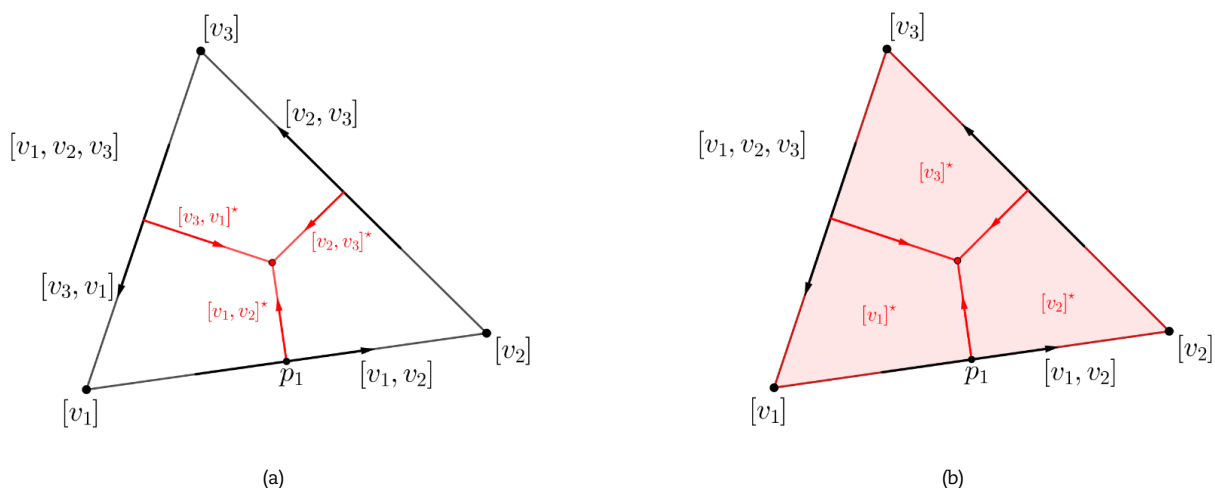


Fig. 4. Oriented 1-dimensional and 2-dimensional dual cells.



### 3. The Convection – Diffusion DEC Discretization

Recall how the 2D isotropic homogeneous stationary Convection-Diffusion eq.(8) reads in Exterior Differential Calculus notation:

$$\star d \star (\underline{u}^\flat \varphi) = \mathbf{k} \star d \star d\varphi + q$$

While it is well known how to discretize the diffusive and source terms (see [22]), the main subject of this paper is the discretization of the transport term.

Note that the operator  $\star d \star$  on the right hand side is applied to a 1-form  $d\varphi$  which will be discretized as a primal 1-form, since the scalar field  $\varphi$  is discretized as a primal 0-form. This indicates to us that the differential 1-form  $\varphi \underline{u}^\flat$  must be discretized as a primal 1-form, i.e. a collection of real values assigned to each oriented edge. In order to do this, it is clear that we can do the following two calculations on a given edge  $[v_i, v_j]$ :

- a) Average the values  $\varphi_i$  and  $\varphi_j$ , i.e.

$$\frac{\varphi_i + \varphi_j}{2}. \tag{20}$$

- b) Integrate  $\underline{u}^\flat$  over the edges of the triangle. Generally, the particle velocity field is sampled at the vertices, so it makes sense assume its discretization at the primal vertices

$$\underline{u} \mapsto \begin{pmatrix} \underline{u}_1 \\ \underline{u}_2 \\ \underline{u}_3 \end{pmatrix}. \tag{21}$$

Now, we interpolate the values of  $\underline{u}$  over the edge  $[v_i, v_j]$  by

$$\underline{u}(s) = \underline{u}_i + \frac{s}{|[v_i, v_j]|} (\underline{u}_j - \underline{u}_i) \tag{22}$$

where  $s \in [0, |[v_i, v_j]|]$ . By using the unit tangent vector  $\underline{T}_{i,j}$ , defined as

$$\underline{T}_{i,j} = \frac{\mathbf{v}_j - \mathbf{v}_i}{|[v_i, v_j]|}, \tag{23}$$

we can express the discretization of  $\underline{u}^\flat$  over the edge  $[v_i, v_j]$  as:

$$\begin{aligned} \tilde{\underline{u}}_{[v_i, v_j]} &:= \int_{[v_i, v_j]} \underline{u}^\flat(\underline{T}_{i,j}) \\ &= \int_0^{|[v_i, v_j]|} \left\{ \underline{u}_i \cdot \underline{T}_{i,j} + \frac{s}{|[v_i, v_j]|} (\underline{u}_j - \underline{u}_i) \cdot \underline{T}_{i,j} \right\} ds \\ &= \frac{\underline{u}_i + \underline{u}_j}{2} \cdot (\mathbf{v}_j - \mathbf{v}_i), \end{aligned} \tag{24}$$

where  $\tilde{\underline{u}}_{[v_i, v_j]}^\flat$  is the discrete value of the primal 1-form on the edge  $[v_i, v_j]$ . As it turns out, it is the inner product of the average of the values of the velocity field at the vertices with the vector given by the oriented edge.

Now, we multiply these two values so that the discretized version of the differential 1-form  $\varphi \underline{u}^\flat$  is

$$\begin{aligned} (\widetilde{\varphi \underline{u}^\flat})_{[v_i, v_j]} &:= \frac{\varphi_i + \varphi_j}{2} \tilde{\underline{u}}_{[v_i, v_j]}^\flat \\ &= \left( \frac{\varphi_i + \varphi_j}{2} \right) \left( \frac{\underline{u}_i + \underline{u}_j}{2} \cdot (\mathbf{v}_j - \mathbf{v}_i) \right). \end{aligned} \tag{25}$$

This definition turns out to coincide with the definition of discrete wedge product of the primal 0-form  $\tilde{\varphi}$  and the primal 1-form  $\tilde{\underline{u}}^\flat$  as defined in [7]. Let:

$$U := -\frac{1}{2} \begin{pmatrix} \tilde{\underline{u}}_{[v_1, v_2]}^\flat & \tilde{\underline{u}}_{[v_1, v_2]}^\flat & 0 \\ 0 & \tilde{\underline{u}}_{[v_2, v_3]}^\flat & \tilde{\underline{u}}_{[v_2, v_3]}^\flat \\ \tilde{\underline{u}}_{[v_3, v_1]}^\flat & 0 & \tilde{\underline{u}}_{[v_3, v_1]}^\flat \end{pmatrix}. \tag{26}$$

Thus, the discretization on the triangle of the 2D isotropic homogeneous stationary Convection-Diffusion equation becomes

$$M_{2,0}(-D_{0,1}^T)M_{1,1}(-U)\tilde{\varphi} = \mathbf{k}M_{2,0}(-D_{0,1}^T)M_{1,1}D_{0,1}\tilde{\varphi} + \tilde{q}, \tag{27}$$

or, equivalently,

$$D_{0,1}^T M_{1,1} (U + \mathbf{k}D_{0,1}) \tilde{\varphi} = M_{0,2} \tilde{q}, \tag{28}$$



where:

$$\tilde{\varphi} = \begin{pmatrix} \varphi_1 \\ \varphi_2 \\ \varphi_3 \end{pmatrix} \quad \text{and} \quad \tilde{q} = \begin{pmatrix} q_1 \\ q_2 \\ q_3 \end{pmatrix}. \tag{29}$$

### 3.1 Transient Problem

The transient isotropic and homogeneous Convection - Diffusion Equation is defined as:

$$\rho \frac{\partial \varphi}{\partial t} + \nabla \cdot (\varphi \underline{u}) = k \nabla^2 \varphi + q \tag{30}$$

where  $\rho$  is a coefficient of the time derivative. We use the following implicit Finite Difference scheme for the discretization of the time derivative, in order to take advantage of the less restrictive time step size:

$$\left[ \frac{\rho}{\Delta t} M_{0,2} + D_{0,1}^T M_{1,1} (U + k D_{0,1}) \right] \tilde{\varphi}^{n+1} = M_{0,2} (\tilde{q} + \frac{\rho}{\Delta t} \tilde{\varphi}^n). \tag{31}$$

## 4. Numerical Experiments

In this section, we show some numerical results on simple domains to show numerical convergence, considering laminar, sinusoidal and rotational velocity fields. The numerical experiments were carried out on a computer with Intel Core i7-7700T with 2.9 GHz CPU and 8 GB of RAM. Gaussian Elimination was used to solve the system of equations obtained from DEC and FEML.

### 4.1 Sinusoidal Flux

For this first example, we consider a rectangular domain under the following conditions (see Fig. 5):

- Diffusion coefficient  $k = 0.05$ .
- Source term  $q = 1$  over disk of radius 0.4 and center in (1,2.5).
- Dirichlet boundary conditions  $\varphi = 0$  over left, upper and bottom boundaries.
- Right boundary with no condition.
- Particle velocity  $\underline{u}(x,y) = (x, \sin(x))$ .

The meshes used for this numerical experiment varies from coarse to fine meshes and are shown in Fig. 6. The approximate DEC-solution for this problem using the mesh shown in Fig. 6(d) has the contour graph shown in Fig. 7.

For comparison purposes, the result obtained with FEML using the finest mesh Fig. 6(d) is considered as the best approximation of the analytical solution. Table 1 shows a comparison of the maximum temperature values obtained with DEC and FEML, the discrepancy (DSP) between the DEC values and those of the best approximation of the analytical solution is also shown, as well as the total execution time.

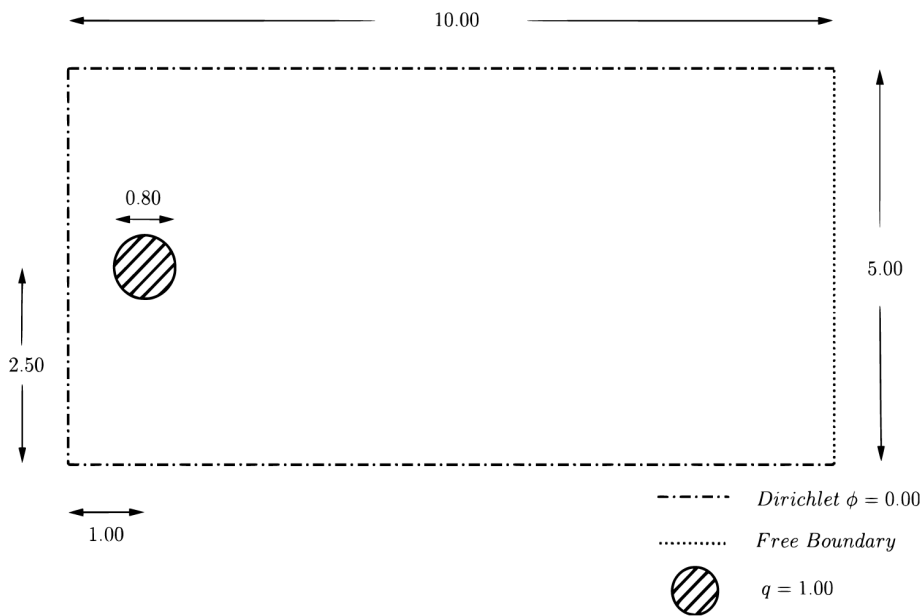


Fig. 5. Domain considered for numerical tests

Table 1. Comparison of the maximum temperature values and assembly times obtained with FEML and DEC in the numerical simulation

Mesh	#Nodes	#Elements	Maximum Temperature Value			Execution Time (sec)	
			FEML	DEC	DSP	FEML	DEC
Fig. 6(a)	687	1272	0.77712	0.77092	0.16716	0.0185	0.020708
Fig. 6(b)	1529	2906	0.68976	0.69538	0.09162	0.093454	0.094232
Fig. 6(c)	5573	10852	0.63237	0.63545	0.03169	1.934143	1.943309
Fig. 6(d)	23351	46100	0.60376	0.60385	9x10 <sup>-5</sup>	78.519231	79.377225



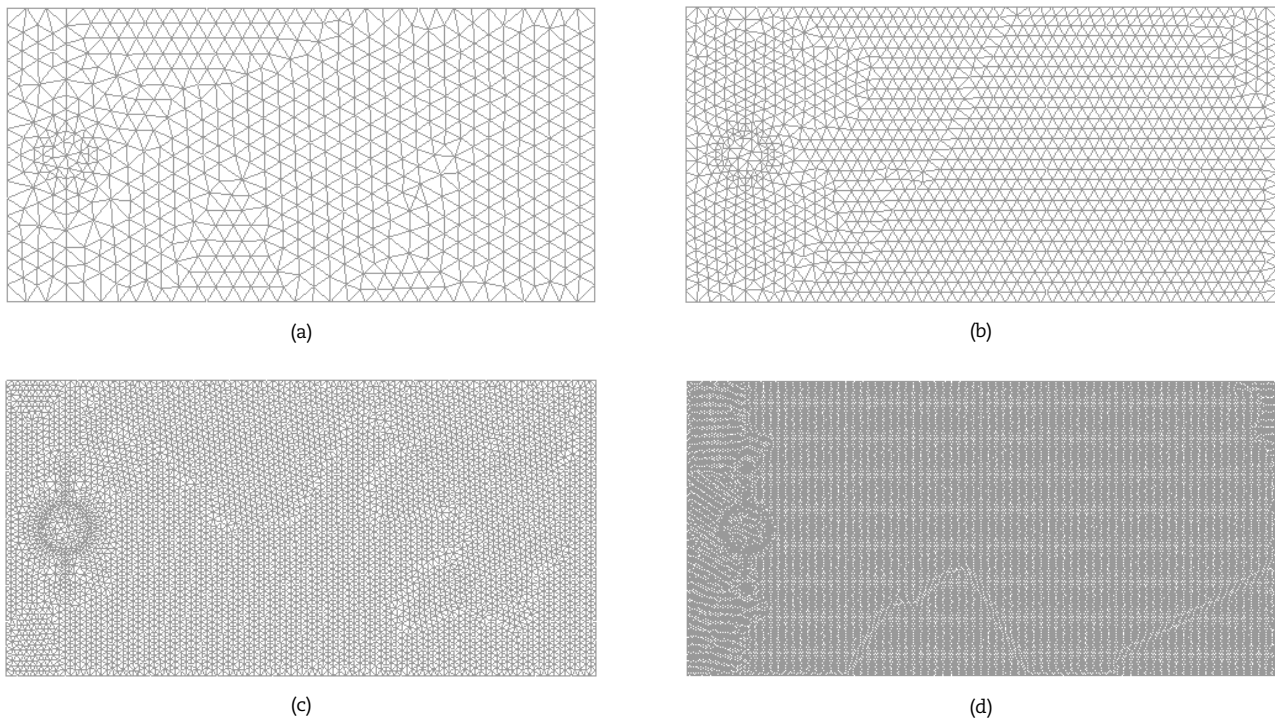


Fig. 6. Meshes used in the numerical simulation

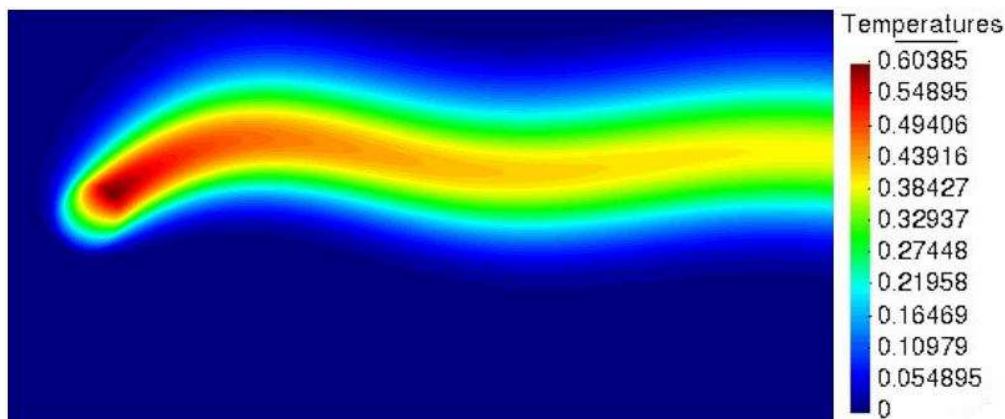


Fig. 7. Solution obtained with DEC using the mesh shown in Fig. 6(d).

Figure 8 shows graphs of temperature values along a central horizontal line of the domain for all meshes as well as a comparison with the best approximation of the analytical solution. This problem is unstable when the meshes shown in Fig. 6(a), Fig. 6(b) and Fig. 6(c) are used to discretize the domain, and small oscillations can be seen in Fig. 8(a) and Fig. 8(b). These oscillations disappear and both numerical methods converge to the same solution when finer meshes are used, as can be seen in Fig. 8.

Nevertheless, given the similarity between DEC and FEML local matrix formulations, a stabilization technique such as the well-known Artificial Diffusion can be introduced to stabilize the problem (see Appendix A), smoothing the solution of both numerical methods. Figure 9 shows a graph of temperature values of the stabilized problem with Artificial Diffusion for the meshes shown in Fig. 6(a), Fig. 6(b) and Fig. 6(c). As can be seen in Fig. 9, most of the oscillations are damped out and similar results are obtained from both FEML and DEC with this stabilization technique.

Figure 10 shows the time evolution of the solution obtained with DEC for the transient problem using the mesh shown in Fig. 6(b). The time-related parameters used for this problem are:

- Time step size  $\Delta t = 0.1$ .
- Final time  $t_f = 5$ .
- Time derivative coefficient  $\rho = 1$ .

Additionally, Fig. 11 shows graphs of the evolution in time of temperature values for different time steps of the transient problem solved with DEC along the same horizontal line as before, and a comparison with the stationary solution is also shown.

As can be seen in Fig. 11, small oscillations are present in each time step, since no stabilization technique was used during this simulation. The solution of the transient problem converges to the same solution of the stationary problem, as expected.



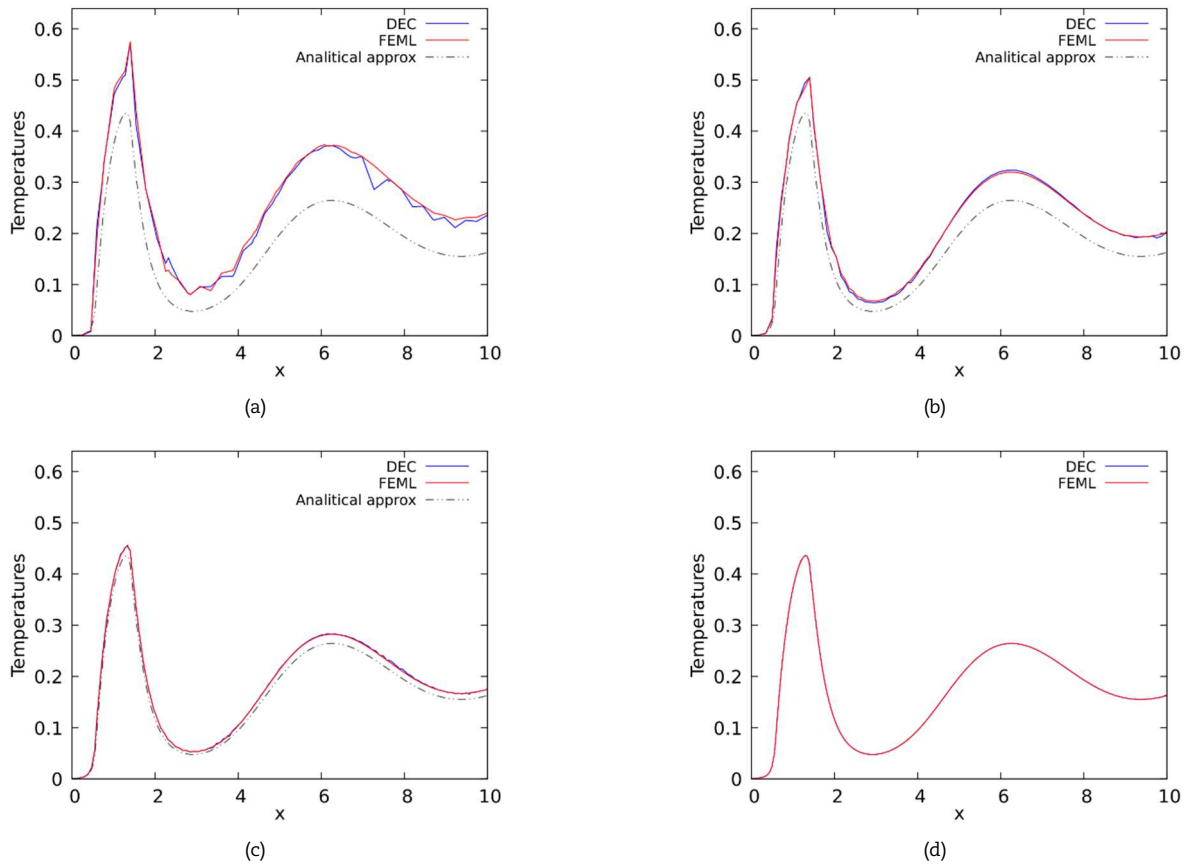


**Fig. 8.** Temperature values along a horizontal section at the center-line of the domain for different meshes. (a) Graph for the mesh in Fig. 6(a); (b) Graph for the mesh in Fig.6(b); (c) Graph for the mesh in Fig. 6(c); (d) Graph for the finest mesh.

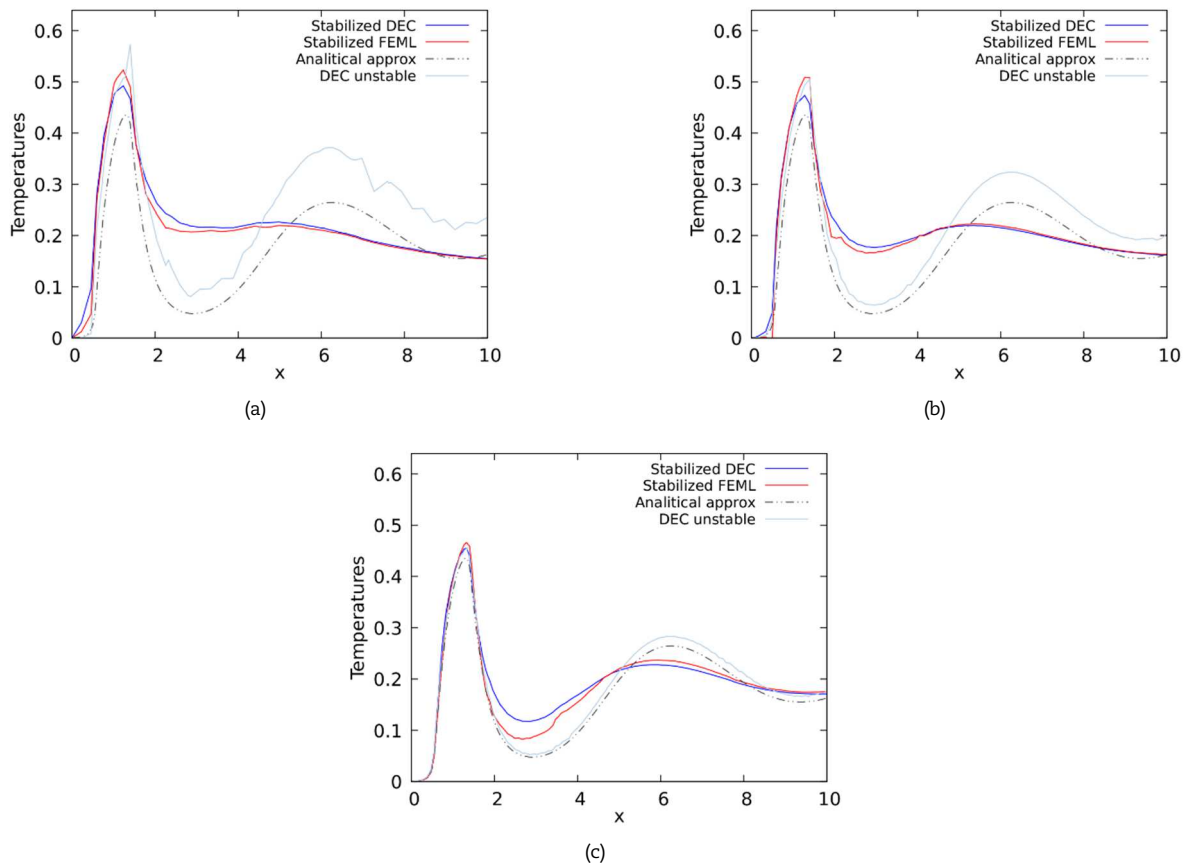


**Fig. 9.** Temperature values of the stabilized problem along a horizontal section at the center-line of the domain for different meshes. (a) Graph for the mesh in Fig. 6(a); (b) Graph for the mesh in Fig 6(b); (c) Graph for the mesh in Fig 6(c).



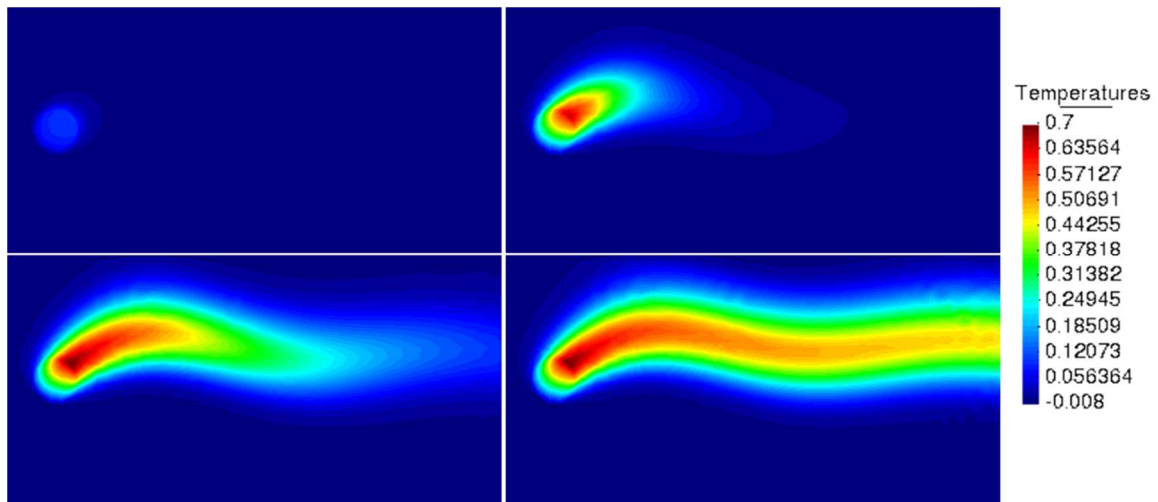


Fig. 10. Contour graphs of the time evolution of the solution obtained with DEC for the transient problem. Times are: t=0.1 (Upper-Left), t=1 (Upper-Right), t=2 (Bottom-Left) and t=4 (Bottom-Right)

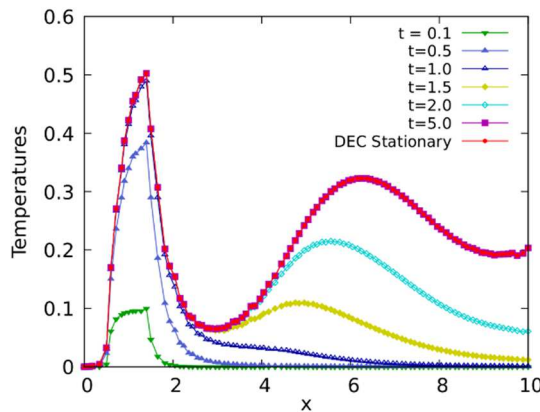


Fig. 11. Temperature values for different time steps for the transient problem obtained with DEC using the mesh shown in Fig. 6(b), along the central horizontal line of the domain.

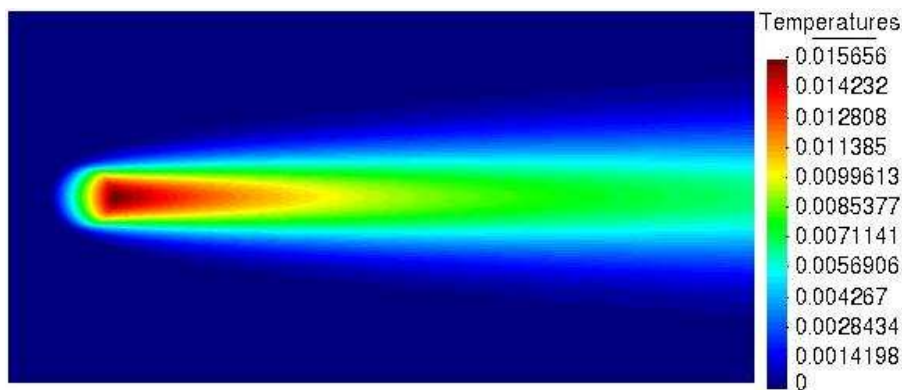


Fig. 12. Solution obtained with DEC using the mesh shown in Fig. 6(d)

4.2 Laminar Flow

For this problem, we considered the same geometry and meshes as the previous example, but now under the following conditions:

- Diffusion coefficient  $k = 1$ .
- Source term  $q = 1$  over disk of radius 0.4 and center in (1,2.5).
- Dirichlet boundary conditions  $\varphi = 0$  over left, upper and bottom boundaries.
- Right boundary with no condition.
- Particle velocity  $\underline{u} = (50,0)$ .

Therefore, this is an incompressible flow problem ( $\nabla \cdot \underline{u} = 0$ ). As before, the solution obtained with FEM using the finest mesh is considered as the best approximation of the analytical solution, for comparison purposes. The solution obtained with DEC using the mesh shown in Fig. 6(d) is shown in Fig. 12.



**Table 2.** Comparison of the maximum temperature values and assembly times obtained with FEMl and DEC in the numerical simulation

Mesh	#Nodes	#Elements	Maximum Temperature Value			Execution Time (sec)	
			FEMl	DEC	DSP	FEMl	DEC
Fig. 6(a)	687	1272	0.019445	0.019847	$4.191 \times 10^{-3}$	0.019546	0.017288
Fig. 6(b)	1529	2906	0.017347	0.017552	$1.896 \times 10^{-3}$	0.095285	0.09365
Fig. 6(c)	5573	10852	0.016301	0.016316	$6.6 \times 10^{-4}$	1.925717	1.943309
Fig. 6(d)	23351	46100	0.015656	0.015656	0	81.754731	82.810216

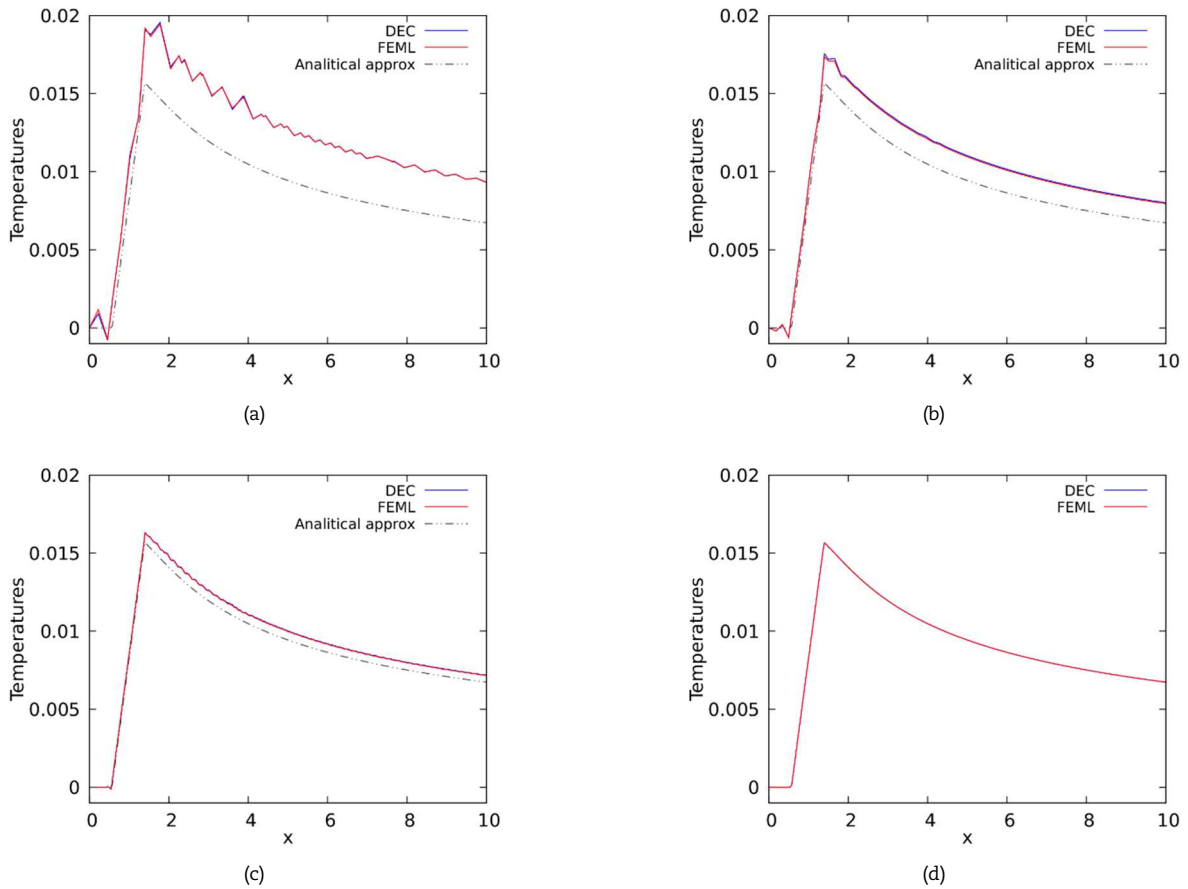


**Fig. 13.** Temperature values along a central horizontal line of the domain for different meshes. (a) Graph for the mesh in Fig 6(a); (b) Graph for the mesh in Fig. 6(b); (c) Graph for the mesh in Fig 6(c); (d) Graph for the finest mesh.

Table 2 shows a comparison of the maximum temperature values obtained with FEMl and DEC for all meshes, the discrepancy value (DSP) between DEC and the best approximation of the analytical solution and the total execution time. Figure 13 shows graphs of the temperature values obtained with DEC and FEMl for all meshes, along a central horizontal line of the domain, and a comparison with the best approximation of the analytical solution.

Again, for the meshes in Fig. 6(a), Fig. 6(b) and Fig. 6(c) both numerical methods are unstable for this problem, as can be seen in Fig. 13(a), Fig. 13(b) and Fig.13(c), where small oscillations are present in the solution. In this example, it is seen that DEC and FEMl behave almost identically for all meshes, as expected, since the gradient of the function obtained with DEC and FEMl coincides (see [21]). As before, Artificial Diffusion can be introduced to avoid the numerical oscillations due to instability. Fig. 14 shows graphs of temperature values of the stabilized problem with Artificial Diffusion.

**4.3 Rotational Velocity Field**

In this example, the domain considered is a disk of radius 2 and center in (0,0) , under the following conditions (see Fig. 15):

- Dirichlet boundary conditions over the perimeter of the disk.
- Source term  $q = 1$  over an internal disk of radius 0.25 and center in (0,1.5).
- Diffusion coefficient  $k = 0.02$  .

Velocity field  $\underline{u} = (y, -x)$  .

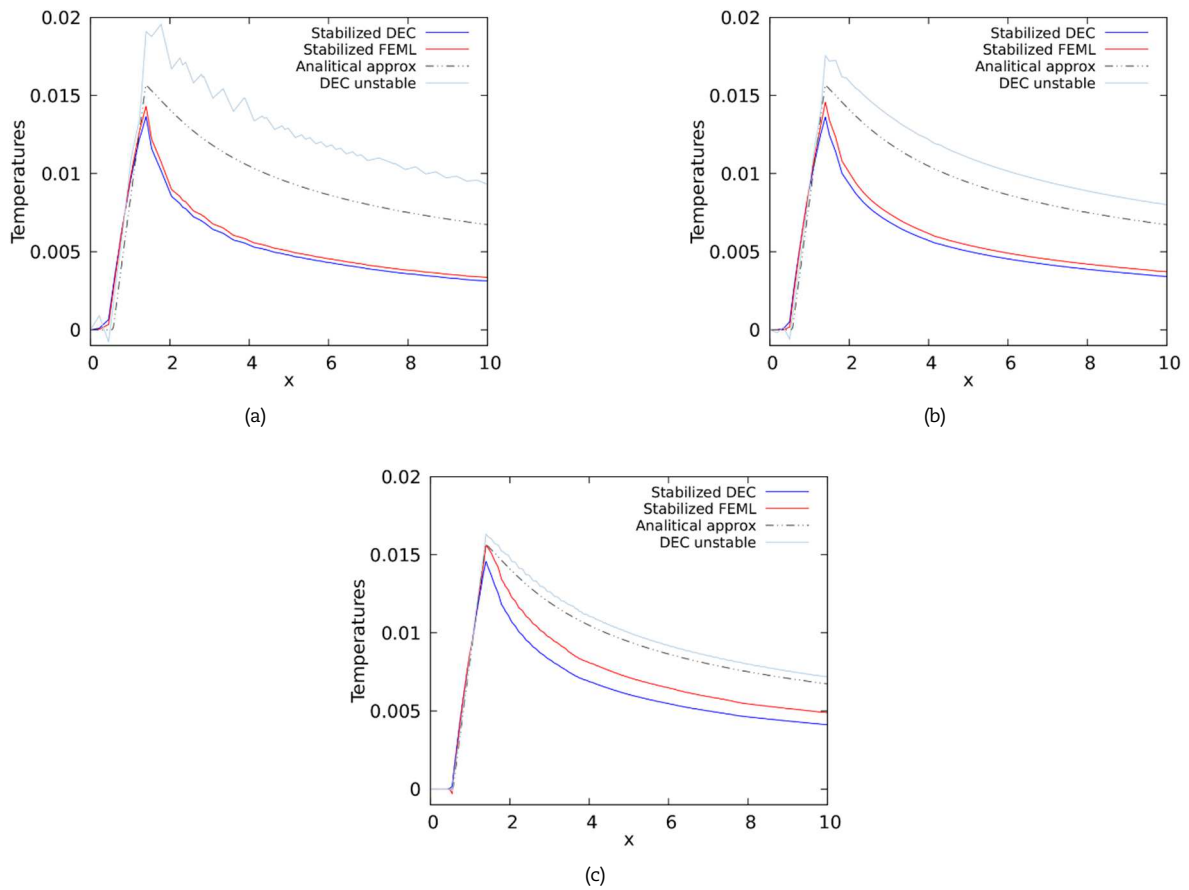
The meshes used in this numerical simulation vary from coarse to fine and are shown in Fig. 16. Again, this is an incompressible flow problem (since  $\nabla \cdot \underline{u} = 0$  ), and the solution obtained with FEMl using the finest mesh (Fig. 16(d)) is taken as the best approximation of the analytical solution.

The solution obtained with DEC using the finest mesh shown in Fig. 16(d) is shown in Fig. 17.

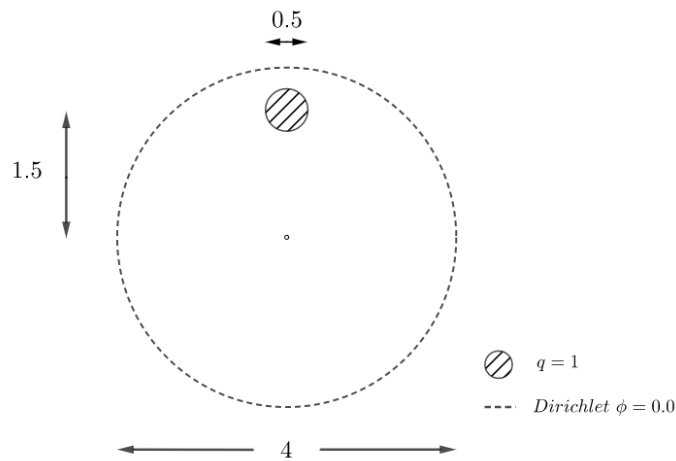
Table 3 shows a comparison of the maximum temperature values obtained with FEMl and DEC for all meshes, the discrepancy between the DEC values and the best approximation of the analytical solution, as well as the total execution time.

Figure 18 shows graphs for the temperature values obtained with DEC and FEMl along a vertical section passing over the center of the domain; and a comparison with the solution obtained with FEMl using the finest mesh, which is taken as the best approximation for the analytical solution, is also shown. This problem is stable for all meshes and no stabilization is required. Like in the previous case, there is a numerical convergence between DEC and FEMl when fine meshes are used.





**Fig. 14.** Temperature values of the stabilized problem along a central horizontal line of the domain for different meshes. (a) Graph for the mesh in Fig. 6(a); (b) Graph for the mesh in Fig. 6(b); (c) Graph for the mesh in Fig. 6(c).



**Fig. 15.** Domain considered for the rotational field example with diffusion coefficient  $k = 0.02$ .

Additionally, Fig. 19 shows the time evolution of the solution obtained with DEC for the transient problem using the mesh shown in Fig. 16(b). The time related parameters are:

- Time step  $\Delta t = 0.2$ .
- Final time  $t_f = 40$ .
- Time derivative coefficient  $\rho = 0.1$ .

**Table 3.** Comparison of the maximum temperature values and assembly times obtained with FEM and DEC in the numerical simulation

Mesh	#Nodes	#Elements	Maximum Temperature Value			Execution Time (sec)	
			FEM	DEC	DSP	FEM	DEC
Fig. 16(a)	687	1272	0.95136	0.99789	0.35247	0.021852	0.021614
Fig. 16(b)	5931	11560	0.68437	0.68646	0.04104	2.301375	2.309375
Fig. 16(c)	11935	23440	0.66832	0.66803	0.02261	14.490640	14.432847
Fig. 16(d)	23351	46100	0.64542	0.6456	$1.8 \times 10^{-4}$	82.128805	80.945272



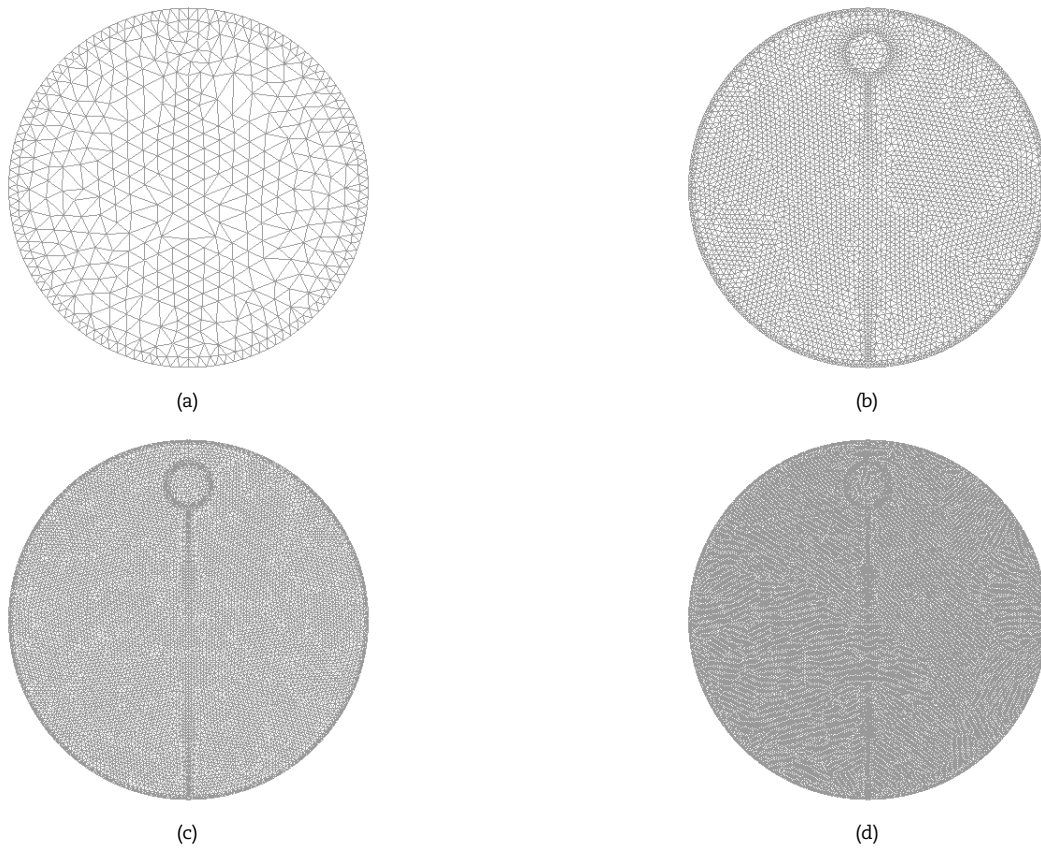


Fig. 16. Meshes used in numerical simulations considering rotational velocity field

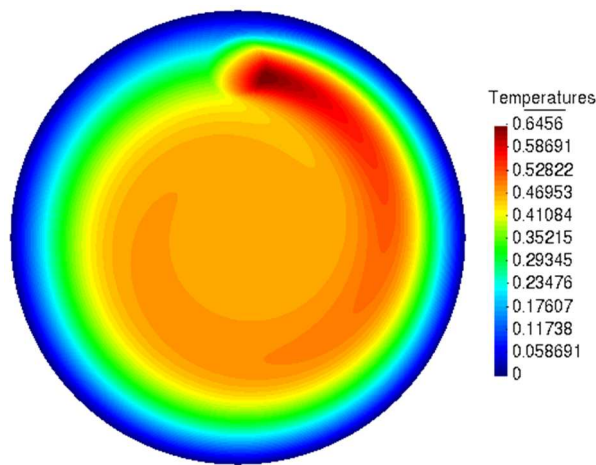


Fig. 17. Solution obtained with DEC using the fines mesh (Fig. 16(d)).

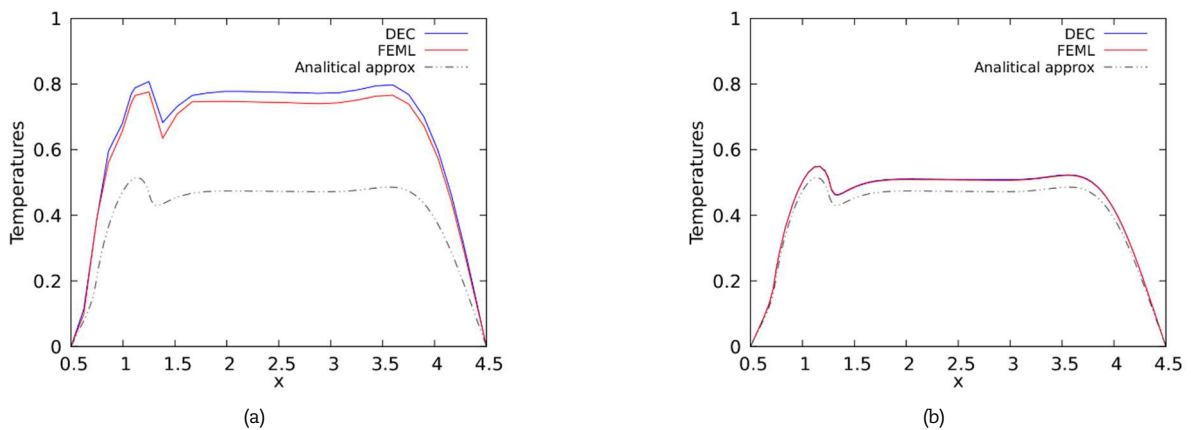


Fig. 18. Temperature values along a vertical section passing over the center of the domain for different meshes. (a) Graph for the mesh in Fig. 16 (a); (b) Graph for the mesh in Fig. 16(b); (c) Graph for the mesh in Fig. 16(c); (d) Graph for the finest mesh.



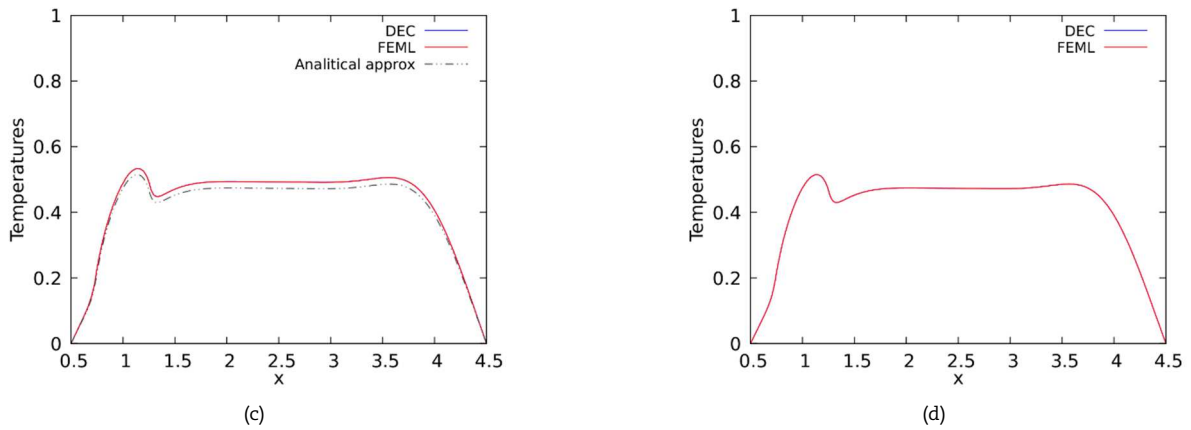


Fig. 18. Temperature values along a vertical section passing over the center of the domain for different meshes. (a) Graph for the mesh in Fig. 16(a); (b) Graph for the mesh in Fig. 16(b); (c) Graph for the mesh in Fig. 16(c); (d) Graph for the finest mesh.

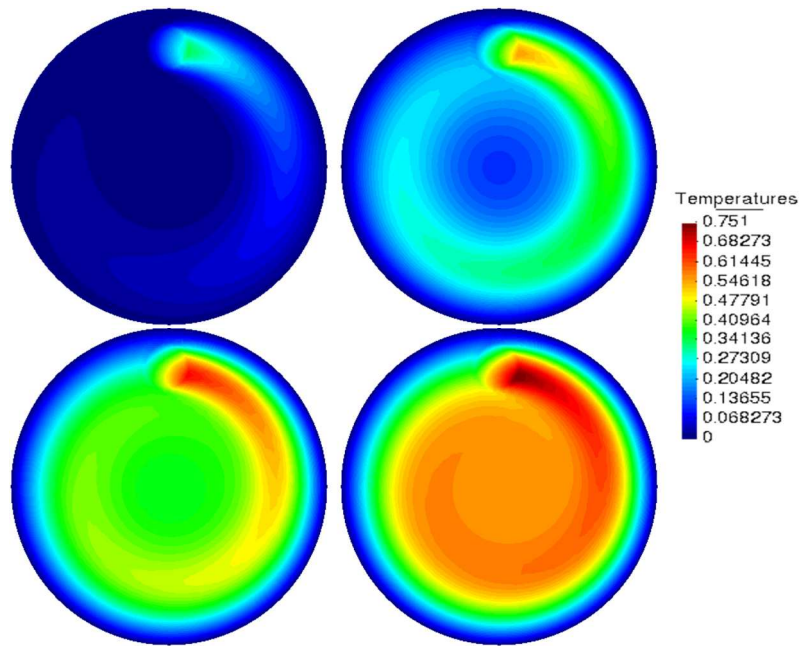


Fig. 19. Contour plots of the temporal evolution of the solution obtained with DEC for the transient problem. Times are:  $t=0.2$  (Upper-Left),  $t=2$  (Upper-Right),  $t=5$  (Bottom-Left) and  $t=36$  (Bottom-right).

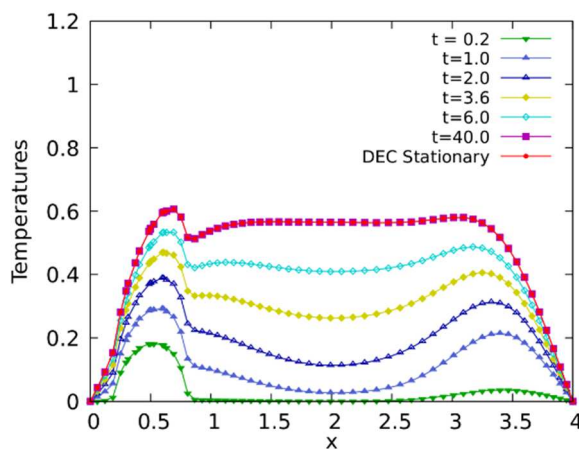


Fig. 20. Temperature values for different time steps of the transient problem obtained with DEC, using the mesh shown in Fig. 16(b), along a vertical section passing through the center of the domain.

Finally, Fig. 20 shows temperature values obtained with DEC along the same section as before, for different time steps of the transient problem, as well as the solution of the transient problem. As can be seen in Fig. 20, the solution of both the transient and stationary problems converge to the same solution.



## 5. Conclusions

We have proposed a local discretization for the convective term of the Convection - Diffusion Equation for compressible and incompressible flow using geometric arguments and known DEC matrix operators for the exterior derivative and the Hodge Star, by considering the velocity field discretized at the primal nodes of the simplicial mesh. By considering the particle velocity discretized in the nodes of the primal mesh and the local formulation of the terms involved, this method is well suited for real applications, since the global system of equations can be assembled using parallel computing and the nodal velocity field obtained with other techniques can be directly plugged-in. Using this feature, the transient problem was formulated using an implicit Finite Difference scheme for the time integration to show numerical convergence to the stationary solution. Our results show similar behavior of our method and FEM for coarse meshes. For finer meshes, both numerical schemes converge to the solution. When convection dominated problems are considered, we have shown that Artificial Diffusion can be introduced to stabilize the solution. Furthermore, no advantage was observed with respect to the execution time of both numerical methods.

## Author Contributions

M.A. Noguez, S. Botello and R. Herrera planned and developed the mathematical model. M.A. Noguez and H. Esqueda designed and developed the software used in the numerical experiments and, together with S. Botello and R. Herrera designed the example problems. All authors participated actively in the development of this work, discussed its contents, results and conclusions and approved the final version of the manuscript.

## Acknowledgments

The third named author would like to thank the International Centre for Numerical Methods in Engineering (CIMNE) and the University of Swansea for their hospitality. We gratefully acknowledge the support of NVIDIA Corporation with the donation of the Titan X Pascal GPU used for this research.

## Conflict of Interest

The authors declared no potential conflicts of interest with respect to the research, authorship and publication of this article.

## Funding

The third and fourth authors were partially supported by a CONACyT grant 256126. The authors received no financial support for the authorship and publication of this article.

## Nomenclature

*	Hodge Star operator	$n$	Mesh dimension
$\Delta t$	Time step	$p$	Permutation variable (equals to $n - 1$ )
$[v_1, v_2, v_3]$	Simplex	$q$	Source term
$[v_i, v_j]$	Edge, $i, j = 1, 2, 3; i \neq j$	$s$	Interpolation variable
$[v_i]$	Vertex, $i=1, 2, 3$	$\underline{u}$	Particle velocity field
$d$	Exterior derivative operator	$U$	Discrete 1-form elemental matrix
$D$	Discrete exterior derivative operator	$u_1, u_2$	Scalar smooth functions
$\det$	Matrix determinant	$v_i$	Point in domain
$k$	Diffusion coefficient	$x, y$	Cartesian coordinates
$M$	Discrete Hodge Star operator	$Y_i, Z_i$	Vector components, $i=1, 2$

## Greek Symbols

$\Omega$	Domain	$\tau$	Line integral variable
$\varphi$	Scalar unknown function	$\rho$	Time derivative coefficient

## Superscripts

$\flat$	Flat operator (transforms vectors to 1-forms)	*	Dual of the cell/discrete operator
$\sim$	Discrete value		

## Appendix

### Artificial Diffusion

The stabilization technique used in this document is based on the one presented in [24]. The isotropic balancing dissipation has the form

$$D^* = \delta \underline{I},$$

where

$$\delta = \alpha \frac{|\underline{u}| h}{2},$$



$\underline{I}$  is the identity tensor and  $|\underline{u}|$  is the magnitude of the mean velocity vector of the element. The magnitude of  $\delta$  and the additional error is determined by the parameter  $\alpha$ . Typically,  $\alpha$  is defined to be a function of the mesh, known as the Peclet number, defined as:

$$P_{e_h} = \frac{|\underline{u}|h}{D},$$

where  $h$  is the local mesh size, which may refer to the longest edge or the diameter of the circumsphere. As a rule of thumb, stabilization is required whenever  $P_{e_h} > 2$  and may take the form:

$$\alpha = \min \left\{ 1, \frac{P_{e_h}}{6} \right\}.$$

As can be seen, artificial diffusion depends only on the mesh size and the PDE's parameters, therefore, its value is independent of the numerical scheme. As stated in [22], the local discretization of the diffusive term with DEC and FEM are roughly identical; this means that the difference between both numerical methods lies in the discretization of the convective term.

## References

- [1] Cartan, E., Sur Certaines Expressions Différentielles et le problème de Pfaff, *Annales Scientifiques de l'École Normale Supérieure*, 16, 1899, 239-332.
- [2] Hirani, A., Discrete Exterior Calculus, Ph.D. Thesis, California Institute of Technology, Pasadena, CA, 2003.
- [3] Douglas, A., Falk, R., Winther, R., Finite Element Exterior Calculus: From Hodge Theory to Numerical Stability, *Bulletin of the American Mathematical Society*, 47, 2010, 281-354.
- [4] Demlow, A., Hirani, A., A Posteriori Error Estimates for Finite Element Exterior Calculus: The de Rham Complex, *Foundations of Computational Mathematics*, 14, 2014, 1337-1371.
- [5] Satoh, T., Yaguchi, T., On the Equivalence of the Norms of the Discrete Differential Forms in Discrete Exterior Calculus, *Japan Journal of Industrial and Applied Mathematics*, 36, 2019, 3-24.
- [6] Hirani, A., Nakshatrala, K., Chaudhry, J., Numerical Method for Darcy Flow Derived Using Discrete Exterior Calculus, *International Journal for Computational Methods in Engineering Science and Mechanics*, 16(3), 2008, 151-169.
- [7] Mohamed, M., Hirani, A., Samtaney, R., Discrete Exterior Calculus of Incompressible Navier - Stokes Equations Over Surface Simplicial Meshes, *Journal of Computational Physics*, 312, 2016, 175 - 191.
- [8] Nitschke, I., Reuther, S., Voigt, A., Discrete Exterior Calculus (DEC) for the Surface Navier-Stokes Equation, Bothe D., Reusken A. (eds) *Transport Processes at Fluidic Interfaces. Advances in Mathematical Fluid Mechanics. Birkhäuser, Cham*, 2017, 177-197.
- [9] Schulz, E., Tsogtgerel, G., Convergence of Discrete Exterior Calculus Approximations for Poisson Problems, *Discrete and Computational Geometry*, 63, 2020, 346-376.
- [10] Dassios, I., Jivkov, A., Abu-Muhari, A., James, P., A mathematical model for plasticity and damage: A discrete calculus formulation, *Journal of Computational and Applied Mathematics*, 312, 2015, 27-38.
- [11] Griebel, M., Rieger, C., Schier, A., Upwind Schemes for Scalar Advection-Dominated Problems in the Discrete Exterior Calculus, Bothe D., Reusken A. (eds) *Transport Processes at Fluidic Interfaces. Advances in Mathematical Fluid Mechanics. Birkhäuser, Cham*, 2017, 145-175.
- [12] Mullen, P., McKenzie, A., Pavlov, D., Durant, L., Tong, Y., Kanso, E., Marsden, J. E., Desbrun, M., Discrete Lie Advection of Differential Forms, *Foundations of Computational Mathematics*, 11, 2011, 131-149.
- [13] Squires, T., Messenger, R. J., Manalis, S. R., Making it Stick: Convection, Reaction and Diffusion in Surface-Based Biosensors, *Nature Biotechnology*, 26(4), 2008, 417-426.
- [14] Giaccherini, A., Al Khatib, M., Cinotti, S., Piciollo, E., Berretti, E., Giusti, P., Innocenti, M., Montegrossi, G., Lavacchi, A., Analysis of mass transport in ionic liquids: a rotating disk electrode approach, *Scientific Reports*, 10(1), 2020, 13433.
- [15] Kim, A. S., Complete Analytic Solutions for Convection-Diffusion-Reaction-Source Equations without using an Inverse Laplace Transform, *Scientific Reports*, 10(1), 2020, 8040.
- [16] Zoppou, C., Knight J. H., Analytical Solutions for Advection and Advection-Diffusion Equations with Spatially Variable Coefficients, *Journal of Hydraulic Engineering*, 123, 1997, 144-148.
- [17] Costa, C., Vilhena, M., Moreira, D., Tirabassi, T., Semi-Analytical Solution of the Steady Three-Dimensional Advection-Diffusion Equation in the Planetary Boundary Layer, *Atmospheric Environment*, 40, 2006, 5659 - 5669.
- [18] Kumar, A., Jaiswal, D. K., Kumar, N., Analytical Solutions to One-Dimensional Advection-Diffusion Equation with Variable Coefficients in Semi-Infinite Media, *Journal of Hydrology*, 380, 2010, 330-337.
- [19] Brooks, A., Hughes, T., Streamline Upwind/Petrov-Galerkin Formulations for Convection Dominated Flows with Particular Emphasis on the Incompressible Navier-Stokes Equations, *Computer Methods in Applied Mechanics and Engineering*, 32, 1982, 199-259.
- [20] Hughes, T., Franca, L., Hulbert, G., A New Finite Element Formulation for Computational Fluid Dynamics: VIII. The Galerkin/Least-Squares Method for Advective-Diffusive equations, *Computer Methods in Applied Mechanics and Engineering*, 73, 1989, 173-189.
- [21] Esqueda, H., Herrera, R., Botello, S., Valero, C., Anisotropy in 2D Discrete Exterior Calculus, *Preprint*, 2018.
- [22] Esqueda, H., Herrera, R., Botello, S., Moreles, M.A., A Geometric Description of Discrete Exterior Calculus for General Triangulations, *Revista Internacional de Métodos Numéricos para Cálculo y Diseño en Ingeniería*, 35(1), 2019, 2.
- [23] Crane, K., de Goes, F., Desbrun, M., Schröder, P., Digital Geometry Processing with Discrete Exterior Calculus, *ACM SIGGRAPH 2013 courses*, California, USA, SIGGRAPH '13, 2013.
- [24] Kusmin, D., A Guide to Numerical Methods for Transport Equations, Friedrich-Alexander-Universität, Erlang-Nürnberg, 2010.

## ORCID iD

Marco A. Noguez  <https://orcid.org/0000-0002-6662-2828>

Salvador Botello  <https://orcid.org/0000-0002-0991-8892>

Rafael Herrera  <https://orcid.org/0000-0001-8393-6573>

Humberto Esqueda  <https://orcid.org/0000-0002-3414-0373>



© 2020 by the authors. Licensee SCU, Ahvaz, Iran. This article is an open access article distributed under the terms and conditions of the Creative Commons Attribution-NonCommercial 4.0 International (CC BY-NC 4.0 license) (<http://creativecommons.org/licenses/by-nc/4.0/>).

How to cite this article: Noguez M.A., Botello, S., Herrera, R., Esqueda, H. Discretization of the Convection-Diffusion Equation Using Discrete Exterior Calculus, *J. Appl. Comput. Mech.*, 6(SI), 2020, 1348-1363. <https://doi.org/10.22055/jacm.2020.34246.2370>

